scientific reports

OPEN

Optimising bifacial dye-sensitized solar cells with graphene-enhanced TPT configuration photoanode for operational stability

Hussein A. AlSultan[1,2]✉, Suhaidi Shafie[1,2]✉, Mohd Nizar Hamidon[1,2], Ismayadi Ismail[2], Shyam S. Pandey[3] & Fauzan Ahmad[4]

Bifacial Dye-sensitized solar cells (bifacial DSSCs) are a promising low-cost and with promising light absorbance alternative to conventional DSSCs, known for their potential for transparency and customizability to be integrated into building-integrated photovoltaic (BIPV). This study explores enhancing efficiency and stability in bifacial DSSCs by integrating graphene into the bifacial configured photoanode. Graphene was incorporated into titanium dioxide (TiO_2) photoanodes using a modified Ti-Nanoxide (T/sp) commercial paste, and powder type (P25) configurate as (T/sp-P25-T/sp) in tri-layer (identified optimal structure to maximizing bifacial light harvesting in our previous study) with Concentrations of 0.05%, 0.1%, and 0.2% graphene were tested. The structural, optical, and electrical properties of the materials were characterised using field emission scanning electron microscopy (FESEM), energy-dispersive X-ray spectroscopy (EDS), Raman spectroscopy, ultraviolet-visible (UV-Vis) spectroscopy, Tauc plots, current-voltage (J-V) measurements, and electrochemical impedance spectroscopy (EIS). The incorporation of 0.1% graphene resulted in the highest initial power conversion efficiency (PCE) of 11.09% under combined front and back illumination at the 4th day of testing, indicating improved electron transport and stability. Over a period of ten days, the performance of these cells remained significantly superior compared to those with pure TiO_2. These results highlight the potential of graphene-enhanced TPT-configured photoanodes for improving both the efficiency and durability of bifacial DSSCs, particularly in applications such as building-integrated photovoltaics.

Keywords Bifacial DSSC, Tri-layer structure, Photoanode, Graphene, Stability

Dye-sensitised solar cells have garnered significant attention due to their low production costs, straightforward fabrication, and abundant, non-toxic materials[1,2]. They are particularly noted for their efficiency under low-light conditions, potential for transparency, and colour customisation, making them a viable alternative to conventional silicon-based photovoltaics. DSSCs consist of a photosensitive dye, a semiconductor (typically Titanium Dioxide or TiO_2), an electrolyte, and counter electrodes. The operational mechanism involves dye molecules absorbing sunlight, exciting electrons from highest occupied molecular orbital (HOMO) to the lowest unoccupied molecular orbital (LUMO) energy state. These electrons are then transferred to the semiconductor's conduction band, circulate through the external circuit, and return at the counter electrode, with electrolyte ions replenishing the dye's electrons to maintain the cell's operational cycle[3,4].

Ruthenium-based complexes are fundamental to DSSCs due to their stability and suitable spectral properties, which, despite having lower molar extinction coefficients compared to typical donor-π-acceptor (D-π-A) organic dyes, still contribute to relatively high PCE and excellent anchoring to TiO_2 particles[5]. The design of these complexes, particularly the donor-π-acceptor, is critical for achieving high efficiencies, reaching up to 14.2% PCE[6]. Platinum (Pt) also plays a crucial role in enhancing DSSC performance through various methods

[1]Institute of Nanoscience and Nanotechnology (ION2), Universiti Putra Malaysia, Jalan UPM, Serdang, Selangor 43400, Malaysia. [2]Faculty of Engineering, Universiti Putra Malaysia, Jalan UPM, Serdang, Selangor 43400, Malaysia. [3]Department of Biological Functions Engineering, Kyushu Institute of Technology, Sensui-cho, Kitakyushu, Fukuoka 804-8550, Japan. [4]Malaysia-Japan International Institute of Technology, Universiti Teknologi Malaysia, Kuala Lumpur, Wilayah Persekutuan 54100, Malaysia. ✉email: GS58052@student.upm.edu.my; hussein.a.alsultan@gmail.com; suhaidi@upm.edu.my

such as doping, Pt-based counter electrodes (CEs), and Pt-decorated reduced graphene oxide (rGO) composites. These approaches have demonstrated improvements in efficiency due to reduced series resistance and enhanced electron transfer rates[7,8].

Despite these advancements, DSSCs' performance is often limited by the electron transport efficiency of TiO_2, which suffers from suboptimal electron-hole separation efficiency[9]. Tailoring the nanostructure and surface chemistry of TiO_2 for example by anodic nanotube growth followed by $TiCl_4$ post-treatment has been shown to lower series resistance and raise PCE by ∼27 %[10]. Similar mobility gains have been reported for cation-doped TiO_2 for instance, Zr-doped nanoparticles used as electron transport layers in perovskite cells cut charge-transfer resistance in half and boost V_{OC} by 70mV[11]. Integrating graphene into TiO_2 matrix has shown promise in addressing these limitations by enhancing electron transport speed and reducing recombination rates, thereby improving photocatalytic activity and light absorption efficiency[12,13].

Stability remains a critical challenge for DSSCs, as dye, electrolyte, and interfacial components degrade over time; recent studies show that encapsulating TiO_2 nanotubes with Cs nanoparticles, for example, can markedly suppress trap states and improve thermal durability[14]. Recent advancements have focused on developing stable materials and electrolyte formulations. For instance, water-containing I^-/I_3^- redox electrolytes have maintained performance and stability even with high water content[15]. Gel polymer electrolytes (GPEs) based on hydroxypropyl cellulose (HPC) and MPII have shown high ionic conductivity and sustained efficiency over long periods[16]. Other studies have used Triton X-100 to improve dye adsorption on TiO_2 photoanodes, enhancing both current short circuit density (J_{SC}) and overall PCE[17]. Comprehensive reviews have identified key factors influencing stability and effective strategies for enhancing DSSC longevity[18].

Bifacial DSSCs, capable of generating electricity from both sides, are notable for their performance under ambient light and aesthetic qualities like transparency and vibrant colours, making them suitable for building-integrated photovoltaics (BIPVs). Innovations in transparent counter electrodes using materials such as PEDOT and Ru-Se alloys have broadened their applicability[19–21]. Graphene, as a doping agent, has the potential to significantly enhance the PCE and durability of DSSCs due to its superior optoelectronic and mechanical properties[22,23]. Its versatility allows it to be used as a cathode support and an anode enhancer, improving electron transfer efficiency[24,25]. However, to our knowledge, integrating graphene in a trilayer structure photoanode in bifacial DSSCs has not yet been investigated. In our previous study[26], a novel approach for bifacial DSSC of trilayer structure has been investigated. The configuration of the Ti-Nanoxide (T/sp) transparent layer for the first and third layers and the TiO_2 variant of (P25) as the light-scattering middle layer has resulted in the highest PCE for bifacial DSSCs due to higher light absorption from both sides. However, electron mobility has yet to be improved in the reported configuration. Modifications of graphene through doping, compositing, and coating with TiO_2 have led to significant performance improvements in DSSCs, which are marked by higher short-circuit current densities and enhanced PCEs. Integrating graphene in bifacial DSSCs could revolutionise back illumination and ambient light harvesting, marking a significant advancement in photovoltaic technology.

Building upon our prior research, this study aims to further enhance the efficiency and stability of DSSCs through strategic modifications to the Stack Formation Framework (SFF) trilayer structure and its configuration of (T/sp-P25-T/sp) or TPT[26]. The primary objectives are to improve electron mobility and enhance overtime working stability. We seek to optimise electron transport and reduce recombination losses by integrating graphene into the TPT configuration. This approach addresses key challenges in light harvesting and electron-hole separation, aiming to significantly improve the operational stability and efficiency of DSSCs under laboratory conditions. Moreover, this work distinguishes itself from previous studies by have doped TiO_2 with graphene to enhance single-side DSSC performance. to our knowledge this is the first demonstration of graphene?enhanced trilayer TPT configuration photoanodes in bifacial DSSCs, achieving over 11% combined PCE and dramatically improved 10-day stability under both front and back illumination.

Materials and method of work

Materials

The materials used in this study were selected based on their established efficacy in DSSC applications. The TiO_2 paste, Transparent Semiconductor Paste Ti-Nanoxide (Product Code: T/sp), and the Pt counter electrodes were sourced from Solaronix, known for their high quality in photovoltaic applications. TiO_2 nanoparticles were obtained as nanopowder (P25) from Degussa and processed into a paste in our lab due to their high surface area and photocatalytic properties. Graphene nanopowder (AO-3: 12nm flakes) nanosheets from graphene Supermarket were chosen for their superior electrical conductivity and large surface area. Transparent conducting oxide (TCO) glass substrates, specifically fluorine-doped tin oxide (FTO) glass with a sheet resistance of 15 Ω/sq, provided a conductive base for the TiO_2 layers. Acetonitrile (solvent), iodine, lithium iodide, 4-tert-butylpyridine, and ethyl-methyl-imidazolium iodide were used for the electrolyte fabrication. All other chemicals, including solvents and reagents, were of analytical grade and used as received without further purification.

Substrate preparation

The FTO glass substrates were prepared by cutting the glass into 2.5 cm x 2 cm dimensions and marking the non-conductive side to ensure proper orientation during subsequent processes. The cleaning process involved an initial rinse with tap water and detergent, followed by a 10-minute ultrasonication to remove any adhered particles. The substrates were then thoroughly rinsed with tap water to remove detergent residues. Following this, a systematic cleaning process using acetone, isopropyl alcohol (IPA), and ethanol was conducted, with each substrate immersed for 15 minutes with the conductive area facing upwards. Post-cleaning, the substrates were air-dried using a stream of hot air and subjected to UV-light treatment to remove any remaining organic residues and enhance the cleanliness of the conductive surface.

TiO_2 paste preparation and graphene doping

In a modification from our last report on SFF[26] in terms of adding graphene as a dopant material to enhance the electrochemical activity of the cell, the fabrication of the photoanode paste began with preparing an ethanol-ethyl cellulose mixture by dissolving 5 grams of ethyl cellulose in 10 mL of ethanol and stirring for two hours. Simultaneously, 1 gram of TiO_2 P25 was heated at 100 °C to remove residual moisture, adding 0.16 mL acetic acid. The mixture was then incrementally combined with 0.8 mL of deionised water and 10 mL of ethanol. Subsequently, another 10 mL of ethanol was pre-mixed with the desired percentage of graphene, and the mixture was ultrasonicated for one hour. Finally, 3.5 mL of α-terpineol was added, and the combined solution was stirred for 12 hours and evaporated until the volume was reduced to one-tenth to achieve the desired paste viscosity for photoanode application.

Electrolyte and counter electrode preparation

The electrolyte for the DSSCs was synthesised using the following components and concentrations: 5 mL of acetonitrile as the solvent, 0.05 M iodine (I_2) corresponding to 64 mg, 0.1 M lithium iodide (LiI) corresponding to 67 mg, 0.5 M 4-test-butyl pyridine (tBP) corresponding to 0.4 mL, and 0.6 M ethyl-methyl-imidazolium iodide (EMII) corresponding to 798 mg. These components were mixed in a 10 mL beaker and stirred using a magnetic stirrer for 15 minutes to ensure complete dissolution and homogeneity[27]. The resulting electrolyte solution was transferred into a well-sealed 10 mL bottle to prevent rapid evaporation. The counter electrodes were prepared using a ready-to-use Pt solution sourced from Solaronix. The preparation involved the following steps: First, the FTO glass substrates were cleaned using the procedure described in the substrate preparation section. The ready-to-use Pt solution was then applied to the cleaned FTO substrates using a spin-coating technique. Fifty microlitres of the Pt solution was spin-coated onto the FTO substrate at 1500 rpm for 10 seconds, followed by annealing at 450 °C for 15 minutes to form a uniform platinum layer on the FTO glass[28].

Modified TPT configuration and DSSC assembly

In the fabrication of the TiO_2 photoanodes, each FTO glass substrate was cleaned, UV-treated, and subjected to a $TiCl_4$ pre-treatment at 80 °C, followed by annealing at 450 °C. A screen-printing technique was used to apply the first TiO_2 layer, confining the active area to 0.25 cm^2, followed by annealing at 450 °C. The resulting mesoporous TiO_2 layer thickness was around 15 µm. This cycle was repeated for each subsequent layer. For the P25 layer, graphene nanopowder was incorporated at concentrations of 0%, 0.05%, 0.1%, and 0.2%. After the final layer, a $TiCl_4$ post-treatment and final annealing at 450 °C were performed to ensure a homogeneous and adherent multi-layered photoanode.

The CEs were prepared from FTO glass with pre-drilled holes. Following the cleaning protocol, the CEs were coated with 50 μL of Pt nanoparticle solution via spin-coating at 1500 rpm for 10 seconds, with a second application after 5 minutes. Post-coating, the electrodes were annealed at 450 °C. The photoanode samples were immersed in a 0.0002 M N719 dye solution in ethanol for 24 hours. Excess dye was removed with ethanol. A 60 μm polymer spacer was placed around the photoanode's active area, and the heated CE was pressed onto the dye-coated photoanode. The electrolyte solution was injected through the pre-drilled holes to complete the assembly.

Electrical characterization

Electrochemical Impedance Spectroscopy (EIS) investigated the charge dynamics within the DSSCs, assessing the impact of structural modifications on charge transfer resistance and recombination rates. J-V (current density-voltage) curve analysis measured the electrical performance of the DSSCs, deriving key performance indicators such as J_{SC}, open-circuit voltage (V_{OC}), fill factor (FF), and overall PCE.

Optical characterization

Ultraviolet-visible (UV-Vis) spectroscopy evaluated the optical properties, focusing on light absorption efficiencies and bandgap shifts induced by graphene doping. This characterisation is essential for understanding the enhancement in the photoanodes' light-harvesting capabilities, directly impacting the DSSCs' performance.

Structural and compositional analysis

Field Emission Scanning Electron Microscopy (FESEM) provided high-resolution visualisations of the surface morphology and cross-sectional architecture, verifying the uniformity and nanostructural integrity of the graphene-doped TiO_2 layers. Energy-dispersive X-ray spectroscopy (EDS) confirmed the elemental composition, ensuring successful graphene integration within the TiO_2 matrix. Raman spectroscopy offered insights into crystalline structure alterations and graphene integration, identifying key peaks corresponding to anatase TiO_2 and graphene and assessing the degree of disorder through the ID/IG ratio, which indicates the level of defects in the graphene structure. X-ray diffraction (XRD) identified the crystalline structures of TiO_2 phases, confirming the presence of anatase TiO_2, which is crucial for photocatalytic activity. This analysis helps understand the structural integrity and phase composition of the graphene-doped TiO_2 layers.

Results and discussion

Electrical characterization

J-V characteristics

To evaluate the performance of the DSSCs, we conducted current-voltage (J-V) measurements under both front and back illumination conditions (AM 1.5 G) solar mass over 10 days. This analysis provides critical insights into the cells' PCE, J_{SC}, V_{OC}, and FF. Tracking these parameters over time allows us to assess the stability and efficiency improvements imparted by different graphene concentrations in the TiO_2 photoanodes. The J-V

Configuration	J_{SC} [mA/cm^2]	V_{OC} [V]	FF	PCE [%]	J_{max} [mA/cm^2]	V_{max} [V]
TPT (Front)	13.13	0.79	0.62	6.40	11.85	0.54
TPT (Back)	6.64	0.77	0.70	3.56	6.14	0.58
$TP_{0.05}T$ (Front)	12.60	0.79	0.61	6.03	11.16	0.54
$TP_{0.05}T$ (Back)	7.16	0.76	0.70	3.81	6.56	0.58
$TP_{0.1}T$ (Front)	12.88	0.78	0.66	6.68	11.72	0.57
$TP_{0.1}T$ (Back)	7.33	0.76	0.65	3.63	6.60	0.55
$TP_{0.2}T$ (Front)	12.84	0.78	0.63	6.29	11.44	0.55
$TP_{0.2}T$ (Back)	6.25	0.77	0.73	3.52	5.87	0.60

Table 1. The front and back illumination of the standard and graphene-enhanced TPT configurations devices by the 10th day.

Day	TPT BFF ratio	$TP_{0.05}T$ Ratio	$TP_{0.1}T$ BFF Ratio	$TP_{0.2}T$ BFF Ratio
1-3 hours	0.619488	0.606183	0.579870	0.424344
Day 1	0.682989	0.713426	0.663732	0.432314
Day 2	0.614823	0.645941	0.619750	0.437583
Day 3	0.682447	0.635098	0.630507	0.492020
Day 4	0.724470	0.606138	0.648635	0.558154
Day 5	0.693359	0.610323	0.629715	0.558347
Day 6	0.663585	0.614538	0.611347	0.558541
Day 7	0.635089	0.618781	0.593515	0.558735
Day 8	0.607817	0.623054	0.576203	0.558929
Day 9	0.581716	0.627356	0.559396	0.559123
Day 10	0.556736	0.631688	0.543079	0.559317

Table 2. Bifaciality factor ratios for different graphene concentrations.

characteristics will enable us to compare the initial performance with the subsequent changes, highlighting the effect of graphene doping on the overall cell efficiency.

TPT Configuration: The performance of DSSCs with the TPT configuration was evaluated under both front and back illumination. The data is presented in Supporting Information Table 1 and Supporting Information Table 2, respectively. On day 0, the test was conducted 1-3 hours after electrolyte injection, with subsequent measurements taken on the following days. The results include initial observed and calculated data using an exponential equation to estimate values for intermediate days.

Under front illumination, Supporting Information Table 1, the highest PCE was observed on day 4, reaching 6.71%. This high efficiency is attributed to the relatively stable values of J_{SC} and V_{OC}, with J_{SC} remaining above 14 mA/cm^2 and V_{OC} around 0.74 V. The FF remained consistent at approximately 0.61. The maximum current density (J_{max}) also showed stability, with values close to 13 mA/cm^2. The high R^2 values for V_{OC} (0.8911) and V_{max} (0.8345) indicate a strong fit of the exponential model, suggesting the robustness of these parameters over the testing period. Figure 1a illustrates the J-V curves for the TPT configuration under front illumination. However, a constant degradation was observed after day 5, with the J_{SC} slowly declining until 13.13 mA/cm^2 with a continuous rise in V_{OC} to nearly 0.8 V at day 10. The increase in V_{OC} DSSCs over time can be attributed to several factors, including structural optimisations[29], interface modifications[30], and the use of specific materials that reduce charge recombination[31]. In some solar cell technologies, such as perovskite solar cells, aging of precursor solutions can lead to a more uniform and smooth film formation, which reduces interfacial gaps and trap state density. This results in an increase in V_{OC} over time, although this specific mechanism is not directly applicable to DSSCs, it highlights the importance of material processing in V_{OC} enhancement[32]. Furthermore, The decline of the data could be from a build-up of resistance in the active area, where the electrolyte influences resistance and performance by affecting ionic mobility, recombination kinetics, and interfacial charge processes within the TiO_2 layer[33,34].

In contrast, under back illumination, as shown in Supporting Information Table 2, the PCE peaked earlier, on day 4, at 4.86%. The J_{SC} values were lower than front illumination, peaking at 10.49 mA/cm^2, consistent with the expected lower efficiency under back illumination. The V_{OC} values were slightly lower, peaking at 0.76 V. The R^2 values for J_{SC} (0.3836) and J_{max} (0.3803) indicate moderate fits, suggesting more variability and potential areas for improvement in the back illumination setup. Figure 2a shows the J-V curves for the TPT configuration under back illumination. Moreover, similar to the front illumination, the back illumination faced a decline in J_{SC}, suggesting steady and constant degradation after day 5.

$TP_{0.05}T$ Configuration: For the $TP_{0.05}T$ configuration, the results under front illumination are shown in the Supporting Information Table 3. The peak PCE of 6.50% was observed on day 2, with a corresponding J_{SC}

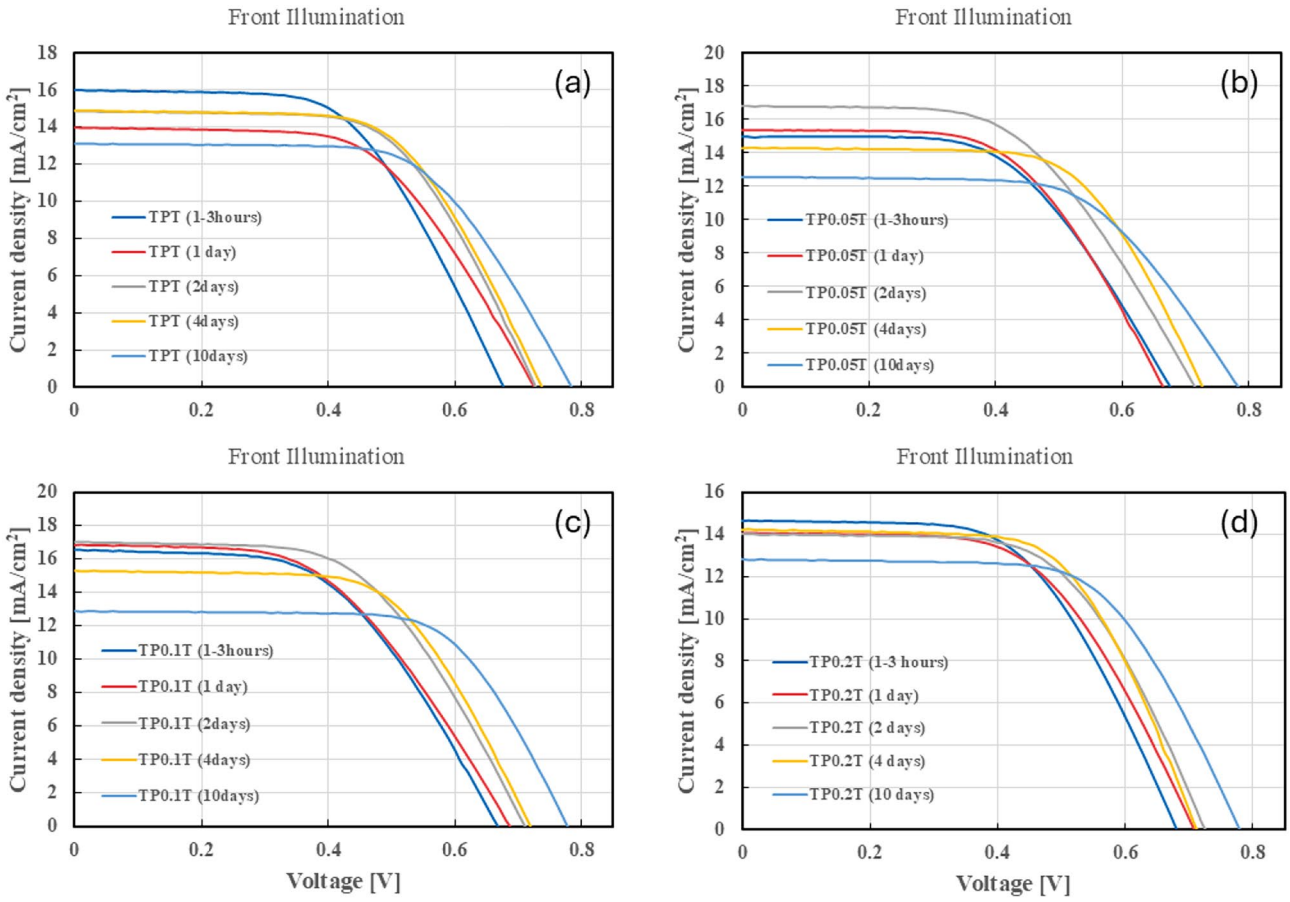

Fig. 1. J-V curves for DSSCs under front illumination conditions over 10 days. The subfigures show the performance of different configurations: (**a**) TPT, (**b**) $TP_{0.05}T$, (**c**) $TP_{0.1}T$, and (**d**) $TP_{0.2}T$. These graphs illustrate the impact of varying graphene concentrations on the stability and efficiency of the cells under consistent front illumination.

of 16.80 mA/cm^2 and V_{OC} of 0.72 V. The FF was relatively high at 0.54, and the J_{max} was 14.44 mA/cm^2. This performance indicates stability enhancement after introducing graphene into the TiO_2 matrix[35]. The R^2 values for J_{SC} (0.7662) and V_{OC} (0.9401) suggest a good fit, indicating consistent performance over time. Figure 1b displays the J-V curves for the $TP_{0.05}T$ configuration under front illumination. The J_{SC} and PCE experienced degradation after day 5, similar to the TPT configuration, suggesting that the graphene percentage is not the optimum quantity needed for further stabilisation.

Under back illumination, as presented in Supporting Information Table 4, the peak PCE was 4.20% on day 2, with the J_{SC} reaching 8.71 mA/cm^2 and the V_{OC} at 0.71 V. The R^2 values for J_{SC} (0.775) and J_{max} (0.7302) indicate a better fit compared to the TPT configuration, suggesting that the $TP_{0.05}T$ configuration may offer more stable performance under back illumination conditions. Figure 2b shows the J-V curves for the $TP_{0.05}T$ configuration under back illumination. The cell remained relatively stable for a couple more days until it started to degrade after day 5.

$TP_{0.1}$**T Configuration:** In the $TP_{0.1}T$ configuration, front illumination results are displayed in Supporting Information Table 5. The highest PCE of 6.73% was observed on day 2, with J_{SC} of 17.04 mA/cm^2 and V_{OC} of 0.71 V. The FF was 0.56, and J_{max} was 14.64 mA/cm^2. The R^2 values for J_{SC} (0.9459) and V_{OC} (0.9794) are exceptionally high, indicating very reliable performance metrics for these parameters. Figure 1c shows the J-V curves for the $TP_{0.1}T$ configuration under front illumination. Although the J_{SC} began to decline after the 3rd to 5th day, the PCE remained stable until day 10 with minimal degradation, suggesting that the 0.1wt% graphene into the TiO_2 greatly enhanced the stability of the cell.

For back illumination, as presented in Supporting Information Table 6, the peak PCE was 4.36% on day 4, with J_{SC} at 9.84 mA/cm^2 and V_{OC} at 0.71 V. The R^2 values for J_{SC} (0.502) and J_{max} (0.4527) indicate a moderate fit, suggesting areas for optimisation in the back illumination performance. The J-V curves for the $TP_{0.1}T$ configuration under back illumination are shown in Figure 2c. The PCE remained relatively above 4% from the 2nd to the 6th day of testing, suggesting a better performance at 0.1wt% graphene than 0.05wt%.

$TP_{0.2}$**T Configuration:** The $TP_{0.2}T$ configuration under front illumination is summarised in Supporting Information Table 7. A peak PCE of 6.29% was achieved on day 4, with J_{SC} of 14.24 mA/cm^2 and V_{OC} of 0.72 V. The FF was 0.61, and J_{max} was 12.84 mA/cm^2. The R^2 values for J_{SC} (0.8682) and V_{OC} (0.9263) indicate

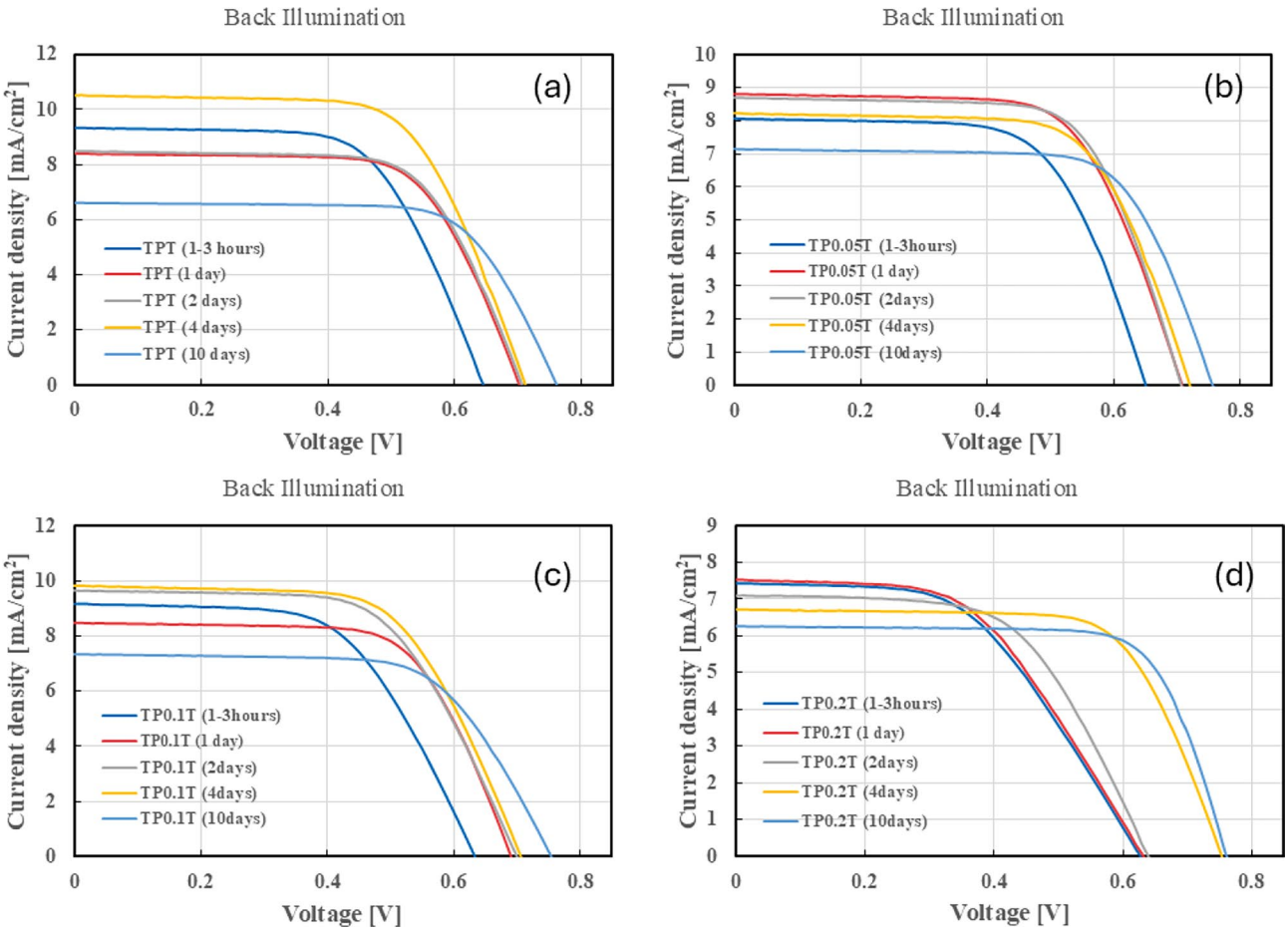

Fig. 2. J-V curves for DSSCs under back illumination conditions over 10 days. The subfigures illustrate the performance variations of different configurations: (**a**) TPT, (**b**) $TP_{0.05}T$, (**c**) $TP_{0.1}T$, and (**d**) $TP_{0.2}T$. These curves highlight the impact of graphene doping on cell efficiency from the rear side of the panels, which is essential for understanding performance under less direct light conditions.

Sample	R_S (Ω)	R_{CT} (Ω)	τ_e (μs)	CPE (nF)	ω_{max} (Hz)	Wo-R (Ω)	Wo-T (ns)	Wo-P
TPT	190.4	45.31	31.8	179.35	4.9142	9.53m	2.28	432.88m
$TP_{0.05}T$	196.2	46.98	50.3	120.62	5.0978	2.77m	0.700	442.19m
$TP_{0.1}T$	190.8	57.44	63.4	19.20	24.1400	1.50m	0.359	450.19m
$TP_{0.2}T$	195.3	59.07	50.3	23.90	25.2220	1.08m	0.237	446.05m

Table 3. Electrochemical parameters from EIS for DSSCs with different graphene concentrations, showing series resistance, charge transfer resistance, electron lifetime, and Warburg parameters.

Sample	Bandgap energy (eV)	Notes
TPT	3.28	Base material
$TP_{0.05}T$	3.27	0.05% graphene doping
$TP_{0.1}T$	3.18	0.1% graphene doping
$TP_{0.2}T$	3.23	0.2% graphene doping

Table 4. Estimated bandgap energies for photoanodes with various graphene concentrations.

Element	Weight %	Atomic %
C K	5.88	10.29
O K	55.45	72.77
Ti K	38.67	16.95
Totals	100.00	-

Table 5. Elemental composition of graphene-doped TiO_2 photoanodes as determined by EDS, showing weight and atomic percentages of carbon (C), oxygen (O), and titanium (Ti).

Peak	k	λ (nm)	β (rad)	θ (rad)	D (nm)
(101)	0.90	0.15	0.03	0.49	6.00
(004)	0.90	0.15	0.05	0.11	2.96
(200)	0.90	0.15	0.03	0.09	4.98
(105)	0.90	0.15	0.05	0.06	2.95
(211)	0.90	0.15	0.03	0.03	4.41

Table 6. Crystallite sizes of $TP_{graphene}T$ photoanodes calculated via the Scherrer equation.

a firm fit, demonstrating stable performance over time. Figure 1d illustrates the J-V curves for the $TP_{0.2}T$ configuration under front illumination. This configuration shows that a higher graphene concentration does not necessarily lead to improved performance, as the J_{SC} and J_{max} declined from the previous concentrations, supporting the finding that 0.1wt% is the optimum concentration for the TPT configuration.

Under back illumination, as detailed in Supporting Information Table 8, the peak PCE was 3.52% on day 6, with J_{SC} at 6.56 mA/cm^2 and V_{OC} at 0.76 V. The R^2 values for J_{SC} (0.9297) and J_{max} (0.9211) suggest a very good fit, indicating that the $TP_{0.2}T$ configuration performs consistently under back illumination conditions. Figure 2d shows the J-V curves for the $TP_{0.2}T$ configuration under back illumination.

The data highlights the enhanced performance and stability of bifacial DSSCs with varying concentrations of graphene under both front and back illumination. The $TP_{0.1}T$ configuration showed the most promising results with the highest R^2 values, suggesting its suitability for further development. The consistent performance under back illumination also indicates the potential for practical applications in environments where both sides of the cell can be exposed to light.

Figure 3 condenses the complete ten-day data set by displaying the arithmetic mean and standard deviation of daily PCE values for each sample. Under front illumination [panel (a)], the $TP_{0.1}T$ device attains the highest time-averaged efficiency of 6.55% ± 0.32%, slightly surpassing the undoped TPT control (6.46% ± 0.24%) and the $TP_{0.05}T$ (6.22% ± 0.30%) and $TP_{0.2}T$ (6.15% ± 0.23%) photoanodes. For back illumination [panel (b)], the ranking is led by TPT at 4.15% ± 0.38%, followed by $TP_{0.1}T$ (3.96% ± 0.28%), $TP_{0.05}T$ (3.92% ± 0.20%), and $TP_{0.2}T$ (3.20% ± 0.45%). These time-averaged results confirm that a 0.1% graphene loading not only yields the highest peak efficiency but also sustains superior front-side performance throughout the entire stability test while maintaining competitive back-side operation.

By the 10th day of the experiment, as shown in Table 1, the results showed a high stability regarding $TP_{0.2}T$ that can be attributed to the high concentration of graphene in the TiO_2 matrix. Similarly, but with higher PCE can be shown in $TP_{0.1}T$. TPT and $TP_{0.05}T$ shown much less stability with higher degradation effect. Summing the front and back illumination efficiencies, the following total PCE values at the 10th day were observed:

- TPT: 9.96% (6.40% + 3.56%)
- $TP_{0.05}T$: 9.84% (6.03% + 3.81%)
- $TP_{0.1}T$: 10.31% (6.68% + 3.63%)
- $TP_{0.2}T$: 9.81% (6.29% + 3.52%)

These findings reinforce the notion that strategic graphene doping can significantly influence the efficacy of bifacial DSSCs, optimising their operational capabilities in varied lighting conditions.

Due to the inherent design of DSSCs, which favours front illumination, the PCE tends to be higher when light is absorbed from the front. This is primarily because the dye molecules, crucial for light harvesting, are more effectively positioned to capture and utilise light entering through the front of the cell[36]. To quantify the performance difference between front and back illumination, we calculate the bifacial factor (BFF) using the formula:

$$\mathrm{BFF} = \frac{\mathrm{PCE_{back}}}{\mathrm{PCE_{front}}}. \tag{1}$$

where $\mathrm{PCE_{back}}$ and $\mathrm{PCE_{front}}$ represent the power conversion efficiencies under the back and front illumination, respectively. This metric helps understand the cell's efficiency from both sides and highlights its potential for varied lighting conditions, particularly in applications where both sides may receive light[37].

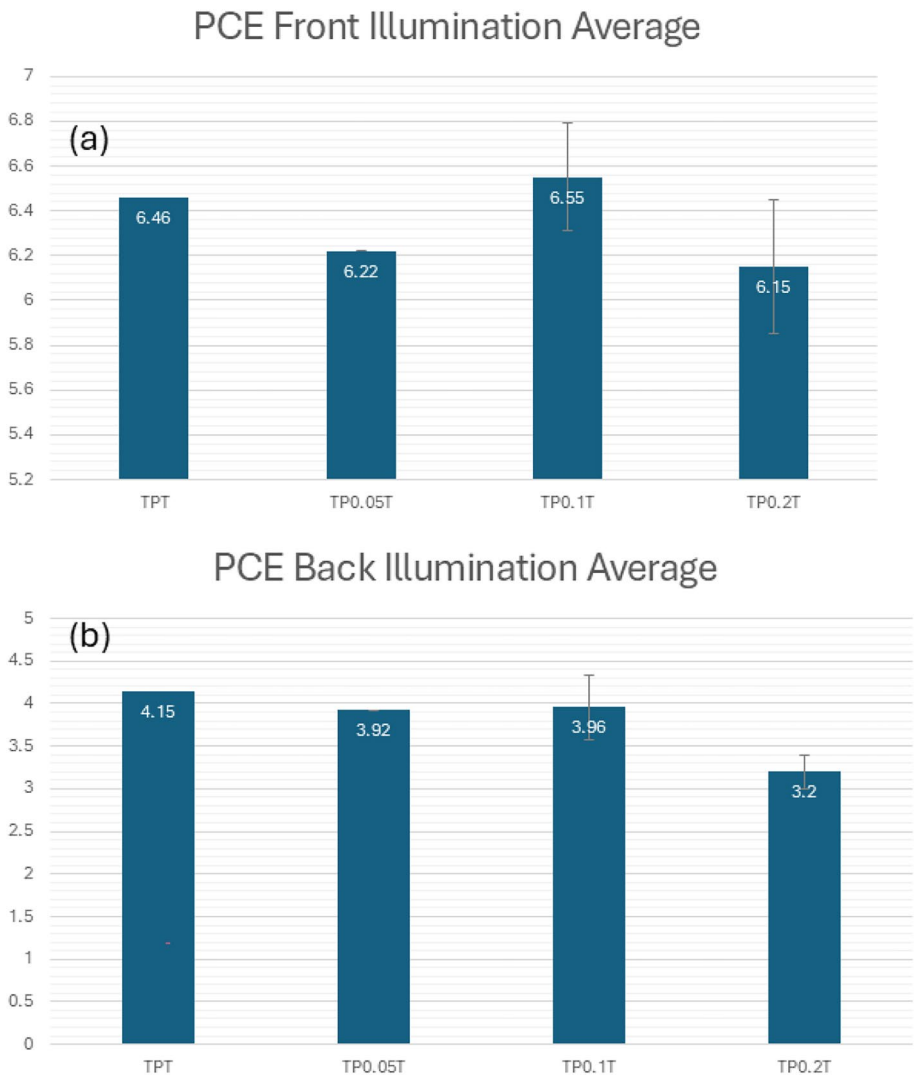

Fig. 3. Time-averaged power conversion efficiency (PCE) of TPT and graphene-doped photoanodes over the full 10-day stability test period under (**a**) front and (**b**) back illumination. Bars represent the mean ± SD (n = 2 pseudo-replicates: front/back measurements of the same device) taken across all measurement days.

The BFF ratios presented in Table 2 reveal significant insights into the performance of DSSCs under different graphene doping conditions. TPT configurations exhibit the highest BFF ratio, peaking at approximately 0.72, indicating a substantial drop in efficiency when transitioning from front-to-back illumination. This trend suggests that while efficient under direct illumination, the standard configuration loses considerable performance when exposed from the rear. The $TP_{0.05}T$ configuration shows a higher maximum BFF ratio of around 0.71, implying a slightly better balance between front and back illumination efficiencies, potentially due to the light scattering effects of the graphene. Notably, the $TP_{0.1}T$ configuration achieves a moderately high ratio but demonstrates more consistency across different measurements, suggesting an optimal graphene concentration for maintaining balance in bifacial applications. Conversely, the $TP_{0.2}T$ configuration consistently shows lower BFF ratios, indicating diminishing returns at higher graphene concentrations, likely due to increased optical density that impedes light penetration to the rear side of the cells. These findings underscore the importance of optimising graphene concentration in the photoanode to achieve a desirable balance between high efficiency and stable bifacial performance.

Analysis of PCE trends over time

The PCE trends were analysed over 10 days to understand the performance and stability of the DSSCs with various graphene concentrations. By plotting the PCE values over time for both front and back illumination, we can observe the peak performance days and the overall stability of the cells. This trend analysis is crucial for identifying the optimal graphene concentration that offers the best balance between initial performance and stability, providing valuable insights into the practical application of these cells in real-world conditions.

For the TPT configuration, the highest front illumination PCE was observed on day 4, reaching 6.71%, while the back illumination PCE peaked on the same day at 4.86%. The $TP_{0.05}T$ configuration showed its highest

front illumination PCE on day 2 at 6.50%, with the back illumination peaking at 4.20% on the same day. The $TP_{0.1}T$ configuration achieved its highest front illumination PCE of 6.73% on day 2, with the back illumination peaking on day 4 at 4.36%. Lastly, the $TP_{0.2}T$ configuration reached its highest front illumination PCE of 6.29% on day 4, while the back illumination peaked on day 6 at 3.52%.

Figure 4 effectively summarises the performance trends, showing each configuration's relative stability and efficiency over time. The consistent performance under back illumination indicates potential for practical applications in environments where both sides of the cell can be exposed to light.

Electrochemical impedance spectroscopy (EIS)

The electrochemical impedance spectroscopy (EIS) analysis revealed that incorporating graphene into TiO_2 photoanodes significantly enhances the electrochemical performance of DSSCs[38]. As illustrated in the Nyquist plots (Figure 5a), the semicircle diameters, which correlate with the charge transfer resistance (Rct), increase with higher graphene content, indicating that while graphene enhances electronic pathways within the TiO_2 matrix, it also introduces interfacial complexities that can hinder charge transfer. The Bode plots (Figure 5b) further support this by showing changes in the phase angle and impedance magnitude, highlighting improved charge separation and electron lifetime, especially in the $TP_{0.1}T$ sample.

Table 3 provides a comprehensive overview of the electrochemical parameters for the different DSSC configurations. The Warburg impedance parameters (Wo-R, Wo-T, and Wo-P) provide insights into the ionic diffusion characteristics within the cells. Lower Wo-R values in the $TP_{0.1}T$ and $TP_{0.2}T$ samples suggest improved ionic diffusion, crucial for efficient dye regeneration and overall device performance. Specifically, the Wo-R value for $TP_{0.1}T$ is 1.50 $\Omega\,S^{-0.5}$, significantly lower than the 9.53 $\Omega\,S^{-0.5}$ observed in the undoped TPT sample. This improvement in ionic transport is corroborated by the enhanced fill factors observed in the J–V characteristics of the graphene-doped DSSCs.

Building on the Warburg analysis, charge-carrier dynamics can be assessed by the electron lifetimes τ_e and corresponding recombination rates

$$k_{\mathrm{rec}} = \frac{1}{\tau_e}.$$

From Table 3, the undoped TPT sample exhibits $\tau_e = 31.8\mu s$, whereas $TP_{0.05}T$, $TP_{0.1}T$, and $TP_{0.2}T$ show extended lifetimes of 50.3µs, 63.4µs, and 50.3µs, respectively. Converting these to recombination rates yields:

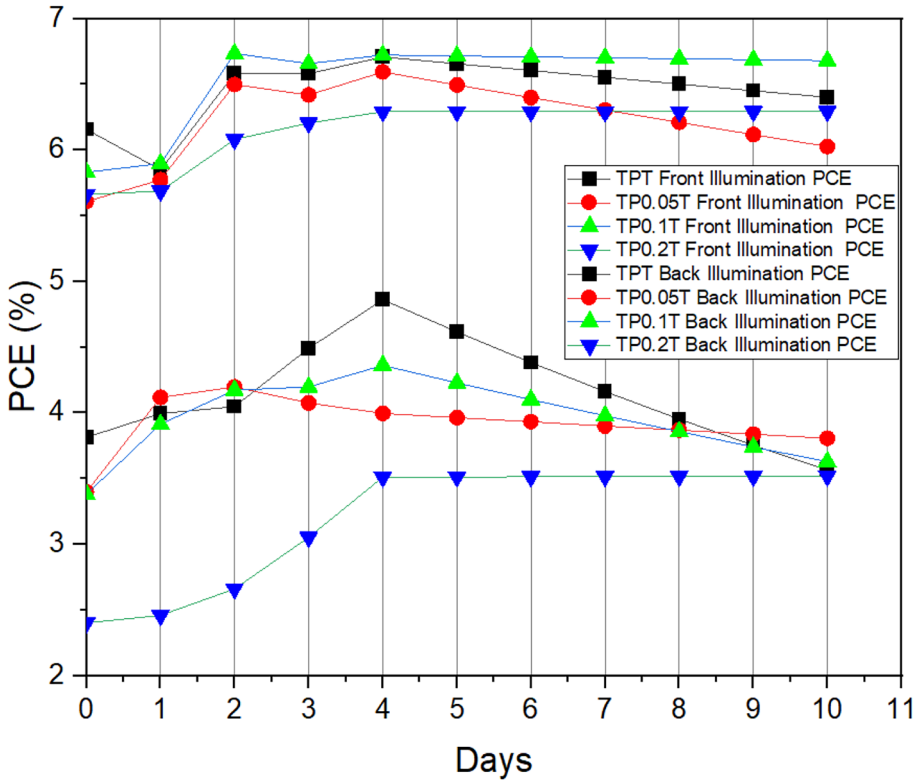

Fig. 4. Power conversion efficiency (PCE) trends over 10 days for DSSCs with varying graphene concentrations under front and back illumination.

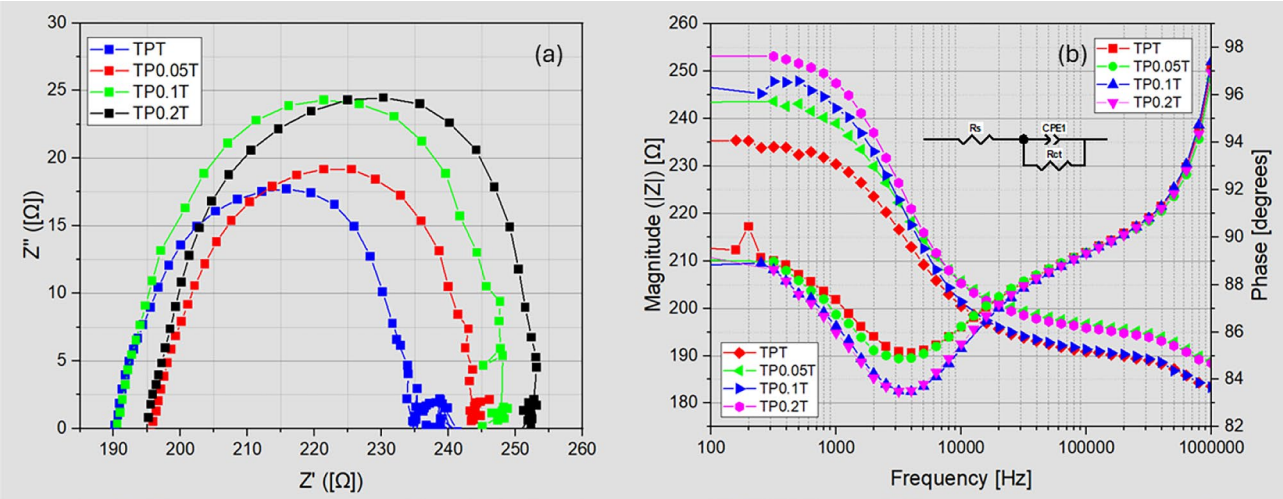

Fig. 5. EIS Nyquist and Bode plots for enhanced TPT with varying graphene concentrations illustrating charge transfer and diffusion characteristics. Panel (**a**) shows Nyquist plots, and panel (**b**) shows Bode plots.

$$k_{\mathrm{rec}} = \frac{1}{\tau_e} \quad \Longrightarrow \quad \begin{cases} k_{\mathrm{rec}}^{\mathrm{TPT}} \approx 3.14 \times 10^4\,\mathrm{s}^{-1}, \\ k_{\mathrm{rec}}^{\mathrm{TP_{0.05}T}} \approx 1.99 \times 10^4\,\mathrm{s}^{-1}, \\ k_{\mathrm{rec}}^{\mathrm{TP_{0.1}T}} \approx 1.58 \times 10^4\,\mathrm{s}^{-1}, \\ k_{\mathrm{rec}}^{\mathrm{TP_{0.2}T}} \approx 1.99 \times 10^4\,\mathrm{s}^{-1}. \end{cases} \tag{2}$$

Notably, the $\mathrm{TP_{0.1}T}$ sample exhibits the longest τ_e and lowest k_{rec}, corresponding to a $\sim 50\%$ reduction in recombination rate compared to undoped TPT. This suppression of carrier recombination underpins the enhanced charge-transfer efficiency. It aligns with the superior PCE and fill factor observed in the J–V characteristics of the $\mathrm{TP_{0.1}T}$ DSSC.

Integrating graphene into $\mathrm{TiO_2}$ photoanodes enhances electronic and ionic transport properties, improving device performance. The optimal concentration of graphene appears to be around 0.1wt%, balancing the benefits of enhanced electron mobility and reduced recombination rates with the complexities introduced at higher doping levels. These findings underscore the potential of graphene-doped $\mathrm{TiO_2}$ photoanodes in advancing the efficiency and stability of DSSCs, making them more viable for practical applications[39].

Optical characterisation: UV-vis absorption spectra and tauc plots

UV-vis absorption spectroscopy was performed to evaluate the optical properties of the graphene-doped $\mathrm{TiO_2}$ samples, and the data were analysed using Tauc plots. UV-vis absorption spectra reveal how adding graphene influences the light absorption capabilities of $\mathrm{TiO_2}$, particularly in the visible region. Derived Tauc plots allow for the estimation of the samples' bandgap energies, which is critical for understanding enhancements in photocatalytic activity and overall cell performance. This optical characterisation helps assess how graphene doping modifies the electronic structure of $\mathrm{TiO_2}$, contributing to improved efficiency in DSSCs[40].

The UV-vis absorption spectra Figure 6 of the graphene-doped $\mathrm{TiO_2}$ samples, measured without dye absorption, illustrates the impact of graphene on the photoanodes' optical properties. For the TPT (undoped $\mathrm{TiO_2}$) sample, the baseline absorption spectrum exhibits typical $\mathrm{TiO_2}$ characteristics with a prominent absorption edge around 380 nm, indicative of its intrinsic bandgap. The $\mathrm{TP_{0.05}T}$ sample shows a slight increase in absorption across the spectrum, suggesting enhanced light-harvesting capabilities due to the presence of graphene. The $\mathrm{TP_{0.1}T}$ sample exhibits a significant increase in absorption in the visible region, indicating that higher concentrations of graphene further improve light absorption properties[41,42]. However, the $\mathrm{TP_{0.2}T}$ sample shows a moderate increase in absorption compared to $\mathrm{TP_{0.05}T}$, but slightly lower than $\mathrm{TP_{0.1}T}$, suggesting an optimal graphene concentration for maximising light absorption.

The Tauc Plots, Figure 7, and Table 4 derived from the UV-vis absorption data provide insights into the optical bandgap energies of the samples. The TPT sample has an optical bandgap of approximately 3.28 eV, consistent with anatase $\mathrm{TiO_2}$. Introducing 0.05% graphene ($\mathrm{TP_{0.05}T}$) slightly decreases the bandgap to 3.27 eV, indicating minor alterations in the electronic structure. An increasingly further reduction to 3.18 eV is observed for the $\mathrm{TP_{0.1}T}$ sample, corresponding to the enhanced visible region absorption seen in the UV-vis spectra, suggesting significant modification of the $\mathrm{TiO_2}$ band structure. The $\mathrm{TP_{0.2}T}$ sample's bandgap slightly increases to 3.23 eV, indicating a saturation point where further graphene addition does not significantly enhance electronic properties and may even slightly decrease performance[43]. These findings confirm that optimal graphene doping can modulate the bandgap of $\mathrm{TiO_2}$, improving light absorption and potential photocatalytic efficiency, which is crucial for optimising graphene concentration in $\mathrm{TiO_2}$ photoanodes for DSSC applications.

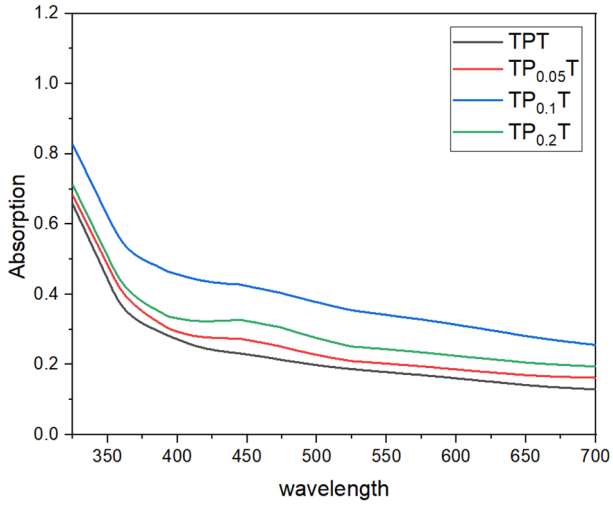

Fig. 6. UV-Vis absorption spectra of undoped and graphene-doped TiO_2 samples indicate the effect of graphene concentration on TiO_2's light absorption properties.

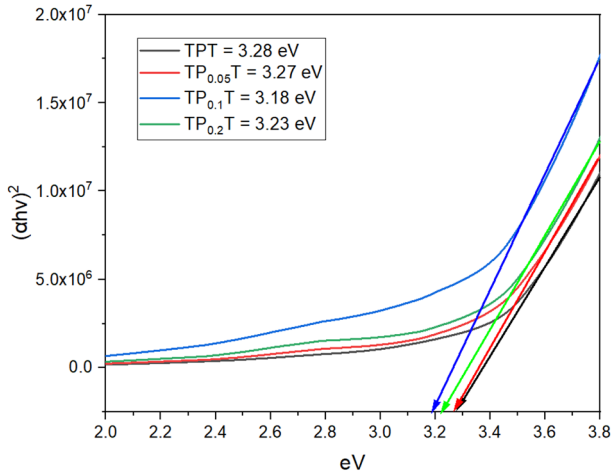

Fig. 7. Tauc plots derived from UV-Vis data for undoped and graphene-doped TiO_2 samples showing bandgap energies that decrease with increasing graphene concentration.

Structural and compositional analysis: FESEM, EDS, XRD, and Raman

To characterise the morphology and elemental composition of the graphene-doped TiO_2 photoanodes, we employed field emission scanning electron microscopy (FESEM) and energy-dispersive X-ray spectroscopy (EDS). The FESEM analysis provides detailed images of the surface structure, allowing us to observe the dispersion and integration of graphene within the TiO_2 matrix. EDS complements this by offering quantitative data on the elemental composition, confirming the presence and distribution of carbon (from graphene), oxygen, and titanium. These techniques help us understand how the structural properties of the photoanodes influence their performance in DSSCs.

The field emission scanning electron microscopy (FESEM)

Figure 8 showcases the surface morphology of the graphene-doped TiO_2 photoanode utilized in our DSSCs. A prominent feature is a distinct graphene nanosheet, measuring approximately 1.77μm by 1.84μm, situated within the TiO_2 matrix. This flat, well-defined structure confirms successful integration of graphene flakes into the semiconductor. The surrounding TiO_2 appears densely packed, with a granular texture typical of nanoparticulate anatase. The contrast between the smooth geometry of the graphene and the granular TiO_2 highlights the heterogeneity introduced by doping, which is expected to improve electron transport and increase surface area for dye adsorption.

From the same FESEM images (see inset of Figure 8), primary TiO_2 particles were measured at 12.4nm, 14.6nm, 20.7nm, 23.3nm and 24.8nm, suggesting a broad size distribution. A quantitative analysis of $n = 100$ particles using ImageJ yields an average diameter of 19.2nm ± 5.4nm (range: 12.4nm to 24.8nm). These SEM-

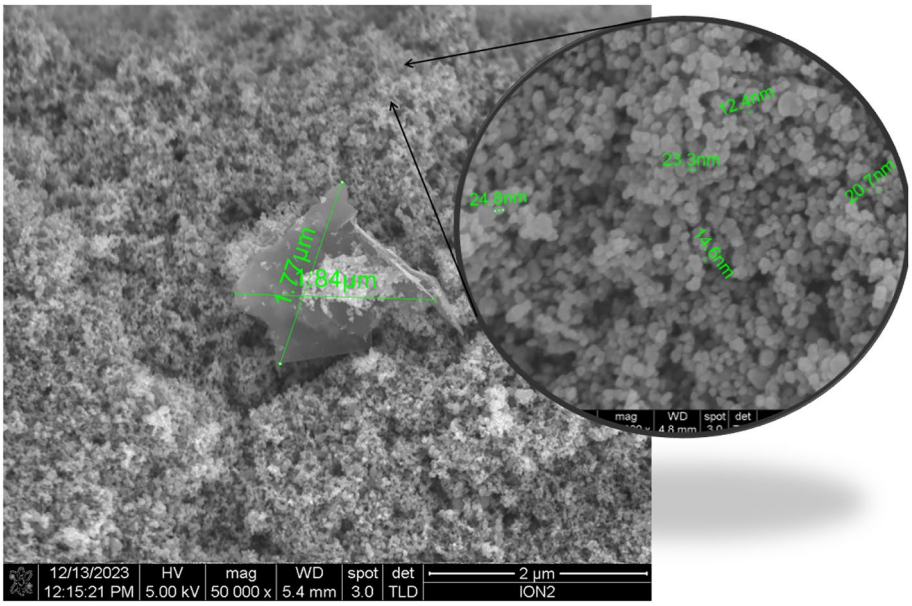

Fig. 8. FESEM image of a graphene-doped TiO_2 photoanode for DSSCs highlighting distinct graphene flakes (approximately 1.77μm by 1.84μm).

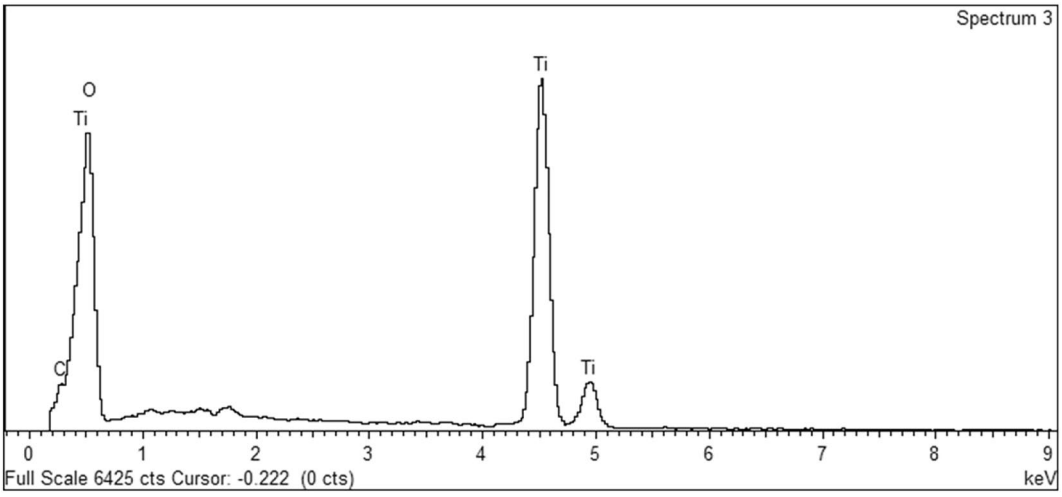

Fig. 9. EDX spectrum of graphene-doped TiO_2 highlighting the peaks corresponding to carbon (C), oxygen (O), and titanium (Ti), indicative of the material's composition.

derived grain sizes exceed the XRD-derived crystallite sizes (4nm to 6nm) obtained from Scherrer analysis (Table 6), indicating that each mesoporous TiO_2 grain comprises multiple smaller anatase domains.

Energy-dispersive X-ray spectroscopy (EDX)

The elemental composition of the graphene-doped TiO_2 photoanodes, pivotal to enhancing the performance of DSSCs, was determined through energy-dispersive X-ray spectroscopy (EDS). As elucidated in Figure 9 and quantitatively summarised in Table 5, the EDS analysis confirmed the presence of carbon (C), oxygen (O), and titanium (Ti) within the samples, with carbon signifying the successful doping of graphene into the TiO_2 matrix. The analysis yielded weight percentages of 5.88% for carbon, 55.45% for oxygen, and 38.67% for titanium, translating to atomic percentages of 10.29%, 72.77%, and 16.95%, respectively. These results verify the incorporation of graphene and underscore the stoichiometric balance of TiO_2 within the composite material. The specific ratios of graphene to TiO_2 offer insights into the doping level, providing a basis for understanding the observed enhancements in photocatalytic activity and photovoltaic performance of the DSSCs. To calculate the atomic weight% between C and Ti :o, we have used a simple equation of C = 10.3 %, Ti:O = 89.7 %, resulting in $\approx$ a 0.115 ratio, which is about 1 C atom for every 8.7 Ti:O atoms.

X-ray diffraction (XRD) analysis

The crystalline structures of the TiO_2 phases in both pure TiO_2 (TPT) and graphene-doped TiO_2 ($TP_{graphene}T$) samples were characterised using X-ray diffraction (XRD). Figure 10 shows the XRD patterns for both samples, highlighting the diffraction peaks corresponding to different crystallographic planes of anatase TiO_2. The peaks are labelled according to their respective planes: (101), (004), (200), (105), and (211). The (101) peak, the most intense and characteristic peak of anatase TiO_2, appears around $2\theta = 25.3^\circ$, confirming the presence of the anatase phase in both samples. The other peaks observed at $2\theta = 37.8^\circ$ (004), 48.0° (200), 53.9° (105), and 62.7° (211) are also consistent with the anatase phase, indicating that the crystalline structure of TiO_2 is maintained upon graphene doping. The intensity of the peaks for the TPT sample is higher than the $TP_{graphene}T$ sample, suggesting that introducing graphene slightly reduces the crystallinity of TiO_2. This reduction in intensity is typical when additional materials like graphene are incorporated into the TiO_2 matrix, as they can introduce some degree of disorder or strain within the crystal structure. However, the preservation of the anatase peaks in the $TP_{graphene}T$ sample indicates that the structural integrity of TiO_2 is primarily maintained even after doping with graphene. The XRD analysis confirms that the predominant phase in TPT and $TP_{graphene}T$ samples is anatase TiO_2. The slight reduction in peak intensity for the graphene-doped sample suggests the successful incorporation of graphene without significantly disrupting the TiO_2 crystal structure.

To further analyse the crystallite sizes of the $TP_{graphene}T$ sample, we have employed Scherrer analysis. D (the diameter) of the photoanodes were extracted from the full-width at half-maximum () of five prominent anatase peaks using the following equation:

$$D = \frac{k\,\lambda}{\beta\,\cos\theta} \tag{3}$$

Crystallite sizes D of the $TP_{graphene}T$ photoanodes were extracted from the full-width at half-maximum (β) of five prominent anatase peaks using the Debye-Scherrer equation (Eq. 3), where k is the shape factor (0.90), λ the X-ray wavelength (0.15?nm), and θ the Bragg angle. As shown in Table 6, the (101) reflection yields the largest crystallite size (6.00?nm), while higher-order reflections such as (004) and (105) give smaller sizes (2.95nm to 2.96nm). The average crystallite size over all five peaks is 4.06 ± 1.17 nm, consistent with a nanocrystalline anatase network that supports efficient dye adsorption and electron transport.

Raman spectroscopy

Raman spectroscopy was utilised to investigate the structural properties and quality of the graphene-doped TiO_2 photoanodes. The Raman spectra provide detailed information on the vibrational modes of the materials, allowing us to identify characteristic peaks of anatase TiO_2 and graphene. The ID/IG ratio, calculated from the Raman spectra, indicates the level of defects and disorder in the graphene structure. This analysis is crucial for understanding the structural integrity and quality of the graphene used in the photoanodes, which directly impact their performance in DSSCs.

The Raman spectroscopic analysis of the graphene-doped TiO_2 photoanodes, integral to our study's DSSCs, reveals critical insights into the composite material's structural properties. As illustrated in Figure 11, distinct peaks corresponding to both the anatase phase of TiO_2 and graphene were identified, confirming the successful integration of graphene. Notably, the anatase TiO_2 peaks at approximately 144 cm^{-1} (*Eg*), 399 cm^{-1} (*B1g*), and 515 cm^{-1} (*A1g/B1g*) indicate the presence of a photocatalytically active anatase phase. The graphene characterisation yielded specific peaks at around 1350 cm^{-1} (*D band*), 1582 cm^{-1} (*G band*), and 2670 cm^{-1} (*2D band*). The ID/IG ratio, calculated as 0.94 from the intensities 529.8 (D) and 502.07 (G), suggests

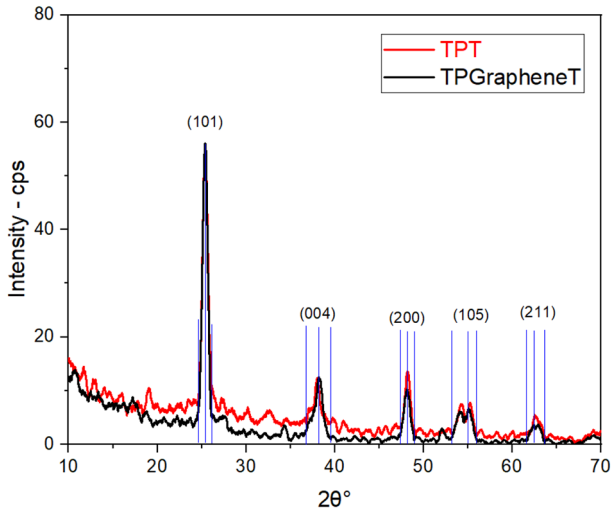

Fig. 10. XRD patterns of TPT (pure TiO_2) and $TP_{graphene}T$ (graphene-doped TiO_2) samples, showing diffraction peaks corresponding to different crystallographic planes of anatase TiO_2.

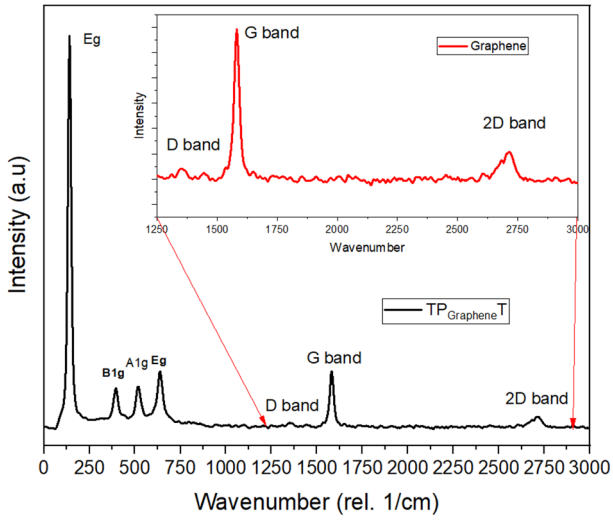

Fig. 11. Raman spectrum of graphene-doped TiO_2 highlighting anatase TiO_2 and graphene peaks.

moderate disorder within the graphene structure. This degree of disorder indicates the presence of defects in graphene, which can enhance photocatalytic activity by providing additional sites for electron trapping, thereby facilitating charge separation and reducing recombination rates. Moreover, the G band's presence confirms the integration of sp^2 carbon atoms, characteristic of graphene's conducive electrical properties. The 2D band, associated with graphene's layered structure, provides insights into the thickness and quality of graphene layers. This comprehensive analysis underscores the synergistic effect between graphene and TiO_2, attributing the observed enhancements in DSSC performance to improved electron mobility and light absorption capabilities.

Thus, the detailed Raman spectroscopy data (Figure 11) not only validate the successful doping of graphene into the TiO_2 matrix but also illuminate how graphene's structural characteristics particularly the moderate disorder signified by the ID/IG ratio contribute to the enhanced efficiency of DSSC. This correlation between graphene's structural properties and DSSC performance underpins the potential of material engineering in advancing photovoltaic technologies.

Conclusion

This study highlights significant advancements in the efficiency and stability of bifacial dye-sensitized solar cells (DSSCs) by incorporating graphene into the SFF configuration of TiO_2 photoanodes. The optimal doping concentration of 0.1 wt% graphene achieved the highest total power conversion efficiency (PCE) of 11.04% under both front and back illumination on the fourth day, and 10.31% after stabilizing on the tenth day. This represents a considerable improvement compared to undoped TiO_2 photoanodes.

Graphene doping enhances stability over time by reducing electron-hole recombination and improving electron transport within the photoanodes. The sample doped with 0.1 wt% graphene ($TP_{0.1}T$) demonstrated high stability along with high efficiency after the initial performance evaluation. Additionally, the short-circuit current density (J_{SC}) for this concentration reached 17.04 mA/cm^2, compared to 15.99 mA/cm^2 for the standard TPT configuration. Moreover, Electrochemical impedance spectroscopy (EIS) confirmed that graphene decreases charge transfer resistance and extends the electron lifetime to 63.4 μs, contributing to the observed improvements. Characterization techniques such as field emission scanning electron microscopy (FESEM), energy-dispersive X-ray spectroscopy (EDS), X-ray diffraction (XRD), and Raman spectroscopy verified the successful integration of graphene into the TiO_2 matrix, maintaining its anatase structure while enhancing electron mobility and light-harvesting capabilities. Furthermore, Ultraviolet-visible (UV-vis) spectroscopy results mirrored the outcomes of the current-voltage (J-V) curve and EIS, showing a reduction in bandgap for the graphene-doped TPT configuration. These findings underscore the potential of graphene-doped TiO_2 photoanodes to advance bifacial DSSC technology, making it viable for practical applications, including building-integrated photovoltaics (BIPVs). Future research should focus on refining the doping process, exploring other doping materials, and conducting long-term performance evaluations in real-world conditions. Overall, doping TiO_2 photoanodes with graphene provides a promising strategy for enhancing the performance of bifacial DSSCs, contributing to the development of highly efficient and durable solar energy conversion devices.

Data availability

The datasets generated and/or analysed during the current study are available from the corresponding author on reasonable request.

Materials availability

All materials used in this study are commercially available and have been described in the methodology section.

Received: 21 March 2025; Accepted: 5 June 2025
Published online: 03 November 2025

References

1. Baby, R., Nixon, P. D., Kumar, N. M., Subathra, M. S. P. & Ananthi, N. A comprehensive review of dye-sensitized solar cell optimal fabrication conditions, natural dye selection, and application-based future perspectives. *Environ. Sci. Pollut. Res.* **29**(1), 371–404. https://doi.org/10.1007/s11356-021-16976-8 (2022).
2. Muñoz-García, A. B. et al. Dye-sensitized solar cells strike back. *Chem. Soc. Rev.* **50**(22), 12450–12550. https://doi.org/10.1039/D0CS01336F (2021).
3. Grätzel, M. Dye-sensitized solar cells. *J. Photochem. Photobiol. C Photochem. Rev.* **4**(2), 145–153. https://doi.org/10.1016/S1389-5567(03)00026-1 (2003).
4. Kalyanasundaram, K. Applications of functionalized transition metal complexes in photonic and optoelectronic devices. *Coord. Chem. Rev.* **177**(1), 347–414. https://doi.org/10.1016/S0010-8545(98)00189-1 (1998).
5. Chou, J.-C. et al. Graphene quantum dots as a co-sensitizer with improving light absorption for dye-sensitized solar cells. *IEEE Trans. Nanotechnol.* **22**, 20–27. https://doi.org/10.1109/TNANO.2023.3235335 (2023).
6. Ji, J., Zhou, H., Eom, Y. K., Kim, C. H. & Kim, H. K. 1.42 % efficiency dye-sensitized solar cells by co-sensitizing novel thieno[3,2-b] indole-based organic dyes with a promising porphyrin sensitizer. *Adv. Energy Mater.* **10**(15), 2000124. https://doi.org/10.1002/aenm.202000124 (2020).
7. Mary, C. I., Senthilkumar, M., Manobalaji, G. & Babu, S. M. Surface-treated cu2znsns4 nanoflakes as pt-free inexpensive and effective counter electrode in dssc. *J. Mater. Sci. Mater. Electron.* **31**(20), 18164–18174. https://doi.org/10.1007/s10854-020-04365-9 (2020).
8. Mujahid, M. & Al-Hartomy, O. A. The effects of pt-doped tio2 nanoparticles and thickness of semiconducting layers at photoanode in the improved performance of dye-sensitized solar cells. *Materials* **15**(22), 7941. https://doi.org/10.3390/ma15227941 (2022).
9. Chou, J.-C. et al. Photovoltaic properties of the titanium dioxide compact layer and reduced graphene oxide for dye-sensitized solar cells under different light intensities. *IEEE J. Photovolt.* **13**(1), 87–94. https://doi.org/10.1109/JPHOTOV.2022.3229189 (2023).
10. Javed, H. M. A. et al. Investigations of anodization parameters and $ticl_4$ treatments on tio_2 nanostructures for highly optimized dye-sensitized solar cells. *Surf. Interfaces* **27**, 101578. https://doi.org/10.1016/j.surfin.2021.101578 (2021).
11. Qureshi, A. A. et al. Incorporation of zr-doped tio_2 nanoparticles in electron transport layer for efficient planar perovskite solar cells. *Surf. Interfaces* **25**, 101299. https://doi.org/10.1016/j.surfin.2021.101299 (2021).
12. Chou, H.-T. et al. Fabrication and properties of graphene electron multiple transporting layers for dye-sensitized solar cell. *IEEE J. Photovolt.* **11**(4), 850–857. https://doi.org/10.1109/JPHOTOV.2021.3075321 (2021).
13. Van Le, C. et al. Rapidly forming the chemical bond titania-carbon in hybrid composite tio2/reduced graphene oxide to enhance the efficiency of dye-sensitized solar cells. *Arab. J. Sci. Eng.* **47**(1), 387–395. https://doi.org/10.1007/s13369-021-05462-5 (2022).
14. Javed, H. M. A. et al. Encapsulation of tio_2 nanotubes with cs nanoparticles to enhance electron injection and thermal stability of perovskite solar cells. *Surf. Interfaces* **23**, 101033. https://doi.org/10.1016/j.surfin.2021.101033 (2021).
15. Park, J., Lee, P., Ko, M. J. Design and fabrication of long-term stable dye-sensitized solar cells: Effect of water contents in electrolytes on the performance. *Int. J. Precis. Eng. Manuf. Green Technol.* **6**(1), 125–131. https://doi.org/10.1007/s40684-019-00025-4 (2019).
16. Ma'alinia, A., Moghaddam, H. A., Nouri, E. & Mohammadi, M. R. Long-term stability of dye-sensitized solar cells using a facile gel polymer electrolyte. *New J. Chem.* **42**(16), 13256–13262. https://doi.org/10.1039/C8NJ02157K (2018).
17. Sonai, G. G., Tiihonen, A., Miettunen, K., Lund, P. D. & Nogueira, A. F. Long-term stability of dye-sensitized solar cells assembled with cobalt polymer gel electrolyte. *J. Phys. Chem. C* **121**(33), 17577–17585. https://doi.org/10.1021/acs.jpcc.7b03865 (2017).
18. Storck, J. et al. Long-term stability improvement of non-toxic dye-sensitized solar cells via poly(ethylene oxide) gel electrolytes for future textile-based solar cells. *Polymers* **12**(12), 3035. https://doi.org/10.3390/polym12123035 (2020).
19. Francis, M. K. et al. Bifacial dssc fabricated using low-temperature processed 3d flower like mos2 - high conducting carbon composite counter electrodes. *Mater. Today Commun.* **27**, 102208. https://doi.org/10.1016/j.mtcomm.2021.102208 (2021).
20. Kang, J. S. et al. Highly efficient bifacial dye-sensitized solar cells employing polymeric counter electrodes. *ACS Appl. Mater. Interfaces* **10**(10), 8611–8620. https://doi.org/10.1021/acsami.7b17815 (2018).
21. Rong, Y., Ku, Z., Li, X. & Han, H. Transparent bifacial dye-sensitized solar cells based on an electrochemically polymerized organic counter electrode and an iodine-free polymer gel electrolyte. *J. Mater. Sci.* **50**(10), 3803–3811. https://doi.org/10.1007/s10853-015-8945-9 (2015).
22. Ngidi, N. P. D., Muchuweni, E. & Nyamori, V. O. Enhanced performance by heteroatom-doped reduced graphene oxide-tio2-based nanocomposites as photoanodes in dye-sensitised solar cells. *Int. J. Energy Res.* **46**(10), 13670–13686. https://doi.org/10.1002/er.8087 (2022).
23. Rahman, M. Y. A. Review of graphene and its modification as cathode for dye-sensitized solar cells. *J. Mater. Sci. Mater. Electron.* **32**(19), 23690–23719. https://doi.org/10.1007/s10854-021-06898-z (2021).
24. Cai, H. et al. Nanostructured composites of one-dimensional tio2 and reduced graphene oxide for efficient dye-sensitized solar cells. *J. Alloys Compd.* **697**, 132–137. https://doi.org/10.1016/j.jallcom.2016.10.189 (2017).
25. Elseman, A. M.: Solar Cells: Theory, Materials and Recent Advances. BoD - Books on Demand (2021). https://doi.org/10.5772/intechopen.87735.
26. AlSultan, H. A. et al. Advancing dye-sensitized solar cell performance with bifacial illumination: A novel stack formation framework approach. *Opt. Mater.* **153**, 115535. https://doi.org/10.1016/j.optmat.2024.115535 (2024).
27. Srivastava, A., Tripathi, M., Awasthi, K. & Banerjee, S. *Materials Science: A Field of Diverse Industrial Applications* (Bentham Science Publishers, 2023).
28. Sangwan, B. et al. Modified poly(vinyl alcohol) based polymer electrolyte for dye sensitized solar cells (dsscs). *Macromol. Symp.* **407**(1), 2100462. https://doi.org/10.1002/masy.202100462 (2023).
29. Jia, H.-L., Zhang, M.-D., Yan, W., Ju, X.-H. & Zheng, H.-G. Effects of structural optimization on the performance of dye-sensitized solar cells: Spirobifluorene as a promising building block to enhance voc. *J. Mater. Chem. A* **4**(30), 11782–11788. https://doi.org/10.1039/C6TA03740B (2016).
30. Neale, N. R. & Kopidakis, N. Tailoring the Interface to Improve Voc in Dye-Sensitized Solar Cells (2005)
31. Abdulkarim, S. S., Hamad, A. E. & Hamad, F. K. Performance improvement of dye sensitized solar cell using vanadium (v) oxide as additives. *Libyan Int. J.* **69**, 4254. https://doi.org/10.37376/glj.vi69.4254 (2023).
32. Guo, Z. et al. Voc over 1.4 v for amorphous tin-oxide-based dopant-free cspbi2br perovskite solar cells. *J. Am. Chem. Soc.* **142**(21), 9725–9734. https://doi.org/10.1021/jacs.0c02227 (2020).
33. Ranjan, R., Aggarwal, S. & Bagga, A. Effect of interfacial resistances at tio2/tco/electrolyte interfaces on dye sensitized solar cells 1–4 (2012). https://doi.org/10.1109/ICEmElec.2012.6636274.
34. Trang, T. T. et al. Effect of conducting ability of electrolytes on the photovoltaic performance of quasi-solid state dye-sensitized solar cells. *Mol. Cryst. Liq. Cryst.* **538**(1), 298–303. https://doi.org/10.1080/15421406.2011.564477 (2011).
35. Razak, M. F. S. A. et al. Graphene-modified tio2 as photoanode using agarose gel electrolyte for dye-sensitized solar cell. *AIP Conf. Proc.* **2496**(1), 020004. https://doi.org/10.1063/5.0091009 (2022).

36. Hora, C., Santos, F., Sales, M. G. F., Ivanou, D. K. & Mendes, A. Conventional and back-illuminated cobalt- and iodine-mediated dye-sensitized solar cells for artificial and solar light conversion. *ACS Appl. Energy Mater.* **5**(12), 14846–14857. https://doi.org/10.1021/acsaem.2c02307 (2022).
37. 7.379 % power conversion efficiency of a numerically simulated solid-state dye-sensitized solar cell with copper (i) thiocyanate as a hole conductor. *East Eur. J. Phys.* 19–31 (2022) https://doi.org/10.26565/2312-4334-2022-3-03.
38. Rajaramanan, T., Heidari Gourji, F., Velauthapillai, D., Ravirajan, P. & Senthilnanthanan, M. Enhanced photovoltaic properties of dye-sensitized solar cells through ammonium hydroxide-modified (nitrogen-doped) titania photoanodes. *Int. J. Energy Res.* **2023**(1), 1090174. https://doi.org/10.1155/2023/1090174 (2023).
39. Fattah, A., Abbasi, A., Bavir, M. & Orouji, A. A. Anode resistance reduction of dye-sensitized solar cells using graphene for efficiency improvement. *Opt. Quantum Electron.* **53**(5), 247. https://doi.org/10.1007/s11082-021-02859-2 (2021).
40. Apostolaki, M.-A. et al. Graphene quantum dot-tio2 photonic crystal films for photocatalytic applications. *Nanomaterials* **10**(12), 2566. https://doi.org/10.3390/nano10122566 (2020).
41. Mehta, M., Chandrabose, G., Krishnamurthy, S., Avasthi, D. K. & Chowdhury, S. Improved photoelectrochemical properties of tio2-graphene nanocomposites: Effect of defect induced visible light absorption and graphene conducting channel for carrier transport. *Appl. Surf. Sci. Adv.* **11**, 100274. https://doi.org/10.1016/j.apsadv.2022.100274 (2022).
42. Özönder, ., Ünlü, C., Güleryüz, C. & Trabzon, L. Doped graphene quantum dots uv-vis absorption spectrum: A high-throughput tddft study. *ACS Omega* **8**(2), 2112–2118. https://doi.org/10.1021/acsomega.2c06091 (2023).
43. Phuthu, L., Dima, R. S., Maluta, N. E., Kirui, J. K. & Maphanga, R. R. Dft study of tio2 brookite (210) surface doped with silver and molybdenum. *Mater. Res. Express* **9**(9), 095901. https://doi.org/10.1088/2053-1591/ac8ae4 (2022).

Acknowledgements
The authors acknowledge the Institute of Nanoscience and Nanotechnology, Universiti Putra Malaysia, and Pandey's Lab, Kyushu Institute of Technology, for providing this study's labs, materials, and equipment. They also extend their appreciation to Universiti Putra Malaysia for the essential assistance via the Geran Putra GP-IPS/2023/9743700.

Author contributions
Hussein A. AlSultan: Conceptualisation, Methodology, Software, Validation, Formal analysis, Investigation, Data Curation, Writing - Original Draft, Writing - Review & Editing, Visualisation. Suhaidi Shafie: Conceptualisation, Resources, Supervision, Project administration, Funding acquisition. Writing - Review & Editing Mohd Nizar Hamidon: Supervision. Ismayadi Ismail: Supervision. Shyam S. Pandey: Resources, Supervision, Project administration, Funding acquisition, Writing - Review & Editing. Fauzan Ahmad: Supervision.

Funding
This research was supported by the Geran Putra GP-IPS/2023/9743700 from Universiti Putra Malaysia.

Declarations

Competing interests
The authors declare no competing interests.

Additional information
Supplementary Information The online version contains supplementary material available at https://doi.org/10.1038/s41598-025-06097-4.

Correspondence and requests for materials should be addressed to H.A.A. or S.S.